Sensors & Actuators: B. Chemical 401 (2024) 135099

Contents lists available at ScienceDirect

Sensors and Actuators: B. Chemical

journal homepage: www.elsevier.com/locate/snb

Soft, conformal PDMS-based ECoG electrode array for long-term in vivo applications

Hyunmin Moon [a,b,1], Jae-Won Jang [a,1], Sumi Park [a,1], Joong-Hyun Kim [c], June Sic Kim [d], Sohee Kim [a,e,*]

[a] Department of Robotics and Mechatronics Engineering, Daegu Gyeongbuk Institute of Science and Technology (DGIST), Daegu 42988, Republic of Korea
[b] Department of Mechanical Engineering, Massachusetts Institute of Technology, Cambridge, MA 02139, USA
[c] Non-Clinical Evaluation Center, Osong Medical Innovation Foundation (KBIOHealth), Cheongju 28160, Republic of Korea
[d] Clinical Research Institute, Konkuk University Medical Center, Seoul 05030, Republic of Korea
[e] Department of Electrical and Computer Engineering, University of California San Diego, La Jolla, CA 92093, USA

ARTICLE INFO

Keywords:
Polydimethylsiloxane (PDMS)
Parylene-treated PDMS
Electrocorticogram (ECoG)
PDMS-based electrodes
Somatosensory evoked potential (SEP)

ABSTRACT

Electrocorticogram (ECoG) electrode arrays based on soft materials, such as polydimethylsiloxane (PDMS), are preferable because they can be implanted with better conformal contact and have physical properties close to biological tissues; thus, the adverse effects on tissues are minimal. However, the realization of electrodes in the micrometer scale on PDMS is challenging. Previously, parylene-treated PDMS was suggested as a solution and proven to be successful in acute in vivo applications. In this study, PDMS-based ECoG electrode arrays fabricated using parylene-treated PDMS (parylene-deposited PDMS and parylene-filled PDMS) are evaluated for the first time in terms of stability and reliability for long-term use. The mechanical and electrochemical properties are investigated over time for up to 8 months through accelerated aging. The ECoG electrode array, implanted in the primary somatosensory area of the brain, can successfully record somatosensory evoked potentials (SEPs) upon mechanical stimulus of the paws with sufficient spatial resolution to distinguish between forepaw and hindpaw stimulations. Finally, the PDMS-based electrodes demonstrate the feasibility of chronic recording for up to 3 months in non-human primates. Based on theses results, it is concluded that they can be used as promising materials and methods to develop various bio-integrated electronic devices that require softness, flexibility, conformability, and robustness over long-term.

1. Introduction

Brain–machine interface (BMI) is a comprehensive term for either a bidirectional or unidirectional passage that allows direct communication between the brain and external equipment [1–4]. At the forefront of BMI, electrodes are used to detect electrophysiological signals by placing them close to the neurons that generate changes in the surrounding electrical potential. Brain activities detected and used for a BMI vary depending on the location of the electrodes [5]. Generally, the more invasive the electrodes, the richer the information in the signal. However, its high invasiveness results in increased foreign body responses, including inflammation and scar tissue formation [6,7]. Electrocorticogram (ECoG) is an electrophysiological signal detected from the cortical surface [8–10]. Over the past few decades, ECoG has been considered a promising method for monitoring brain activity with higher spatial and temporal resolutions compared with electroencephalography (EEG); additionally, it is less invasive than intracortical electrodes [11,12].

The stable use of an ECoG electrode array requires mechanical properties similar to those of biological tissues in in vivo environments [13–15]. The substrate material of electrodes with high stiffness can cause the formation of scar tissue surrounding the electrodes, thereby deteriorating the recording performance [16,17]. Polydimethylsiloxane (PDMS) is preferred for implantable devices owing to its flexibility, stretchability, optical transparency and biocompatibility [18–23]. In particular, it has Young's modulus ranging from 360 to 870 kPa [24],

* Corresponding author at: Department of Robotics and Mechatronics Engineering, Daegu Gyeongbuk Institute of Science and Technology (DGIST), Daegu 42988, Republic of Korea.
E-mail address: soheekim@dgist.ac.kr (S. Kim).
[1] These authors contributed equally to this work.

https://doi.org/10.1016/j.snb.2023.135099
Received 31 August 2023; Received in revised form 14 November 2023; Accepted 1 December 2023
Available online 4 December 2023

significantly lower than those of polyimide or parylene (~ 3.2 GPa [25]) that have been more frequently used in ECoG electrodes. Considering the Young's modulus of the brain, which ranges from 1 to 30 kPa, PDMS is certainly a good candidate for substrate materials. Though micro-cracks in the deposited metal layers on native PDMS substrate are inevitable, two types of parylene-treated PDMS have been introduced to overcome this challenge by employing parylene-C (hereinafter, also referred to as 'parylene'): parylene-deposited PDMS and parylene-filled PDMS [26–29]. Parylene-deposited PDMS is generated through chemical vapor deposition of parylene with a thickness of submicrometers on the PDMS, whereas parylene-filled PDMS is generated by further processing the parylene-deposited PDMS such that the deposited parylene layer is fully etched from the surface of the PDMS, leaving parylene residues only filled inside the nanopores of the PDMS surface (Fig. 1a). Using these two parylene-treated PDMS substrates, soft and flexible electrodes have been fabricated with crack-free and reliable metal patterns on PDMS-based substrates while maintaining the flexible and stretchable characteristics of PDMS preserved [27,30,31].

As more attention is attracted to utilizing soft, flexible and stretchable PDMS for implantable devices, the long-term usability of PDMS-based bioelectronic devices in in-vivo environments becomes of great interest. A few research groups have paid attention to using PDMS as the substrate material of ECoG electrodes [20–22,30]. Unlike other PDMS-based ECoG electrodes, the fabrication of electrodes based on parylene-treated PDMS can employ almost all micro-electromechanical systems (MEMS) processes such as sputter deposition and lithographical patterning on the soft and flexible substrate, as can be done on a single silicon wafer [30]. ECoG recordings using previously developed PDMS-based electrodes were reported from acute recordings to for periods of 6 weeks up to 3 months. However, none of them reported the quantitative analysis of temporal changes in device characteristics associated with signal quality over time. Consequently, the long-term stability and reliability of PDMS-based bioelectronic devices, in particular, devices based on parylene-treated PDMS, in wet and ionic environments has not yet been demonstrated to date.

In this study, we systematically investigated the long-term stability

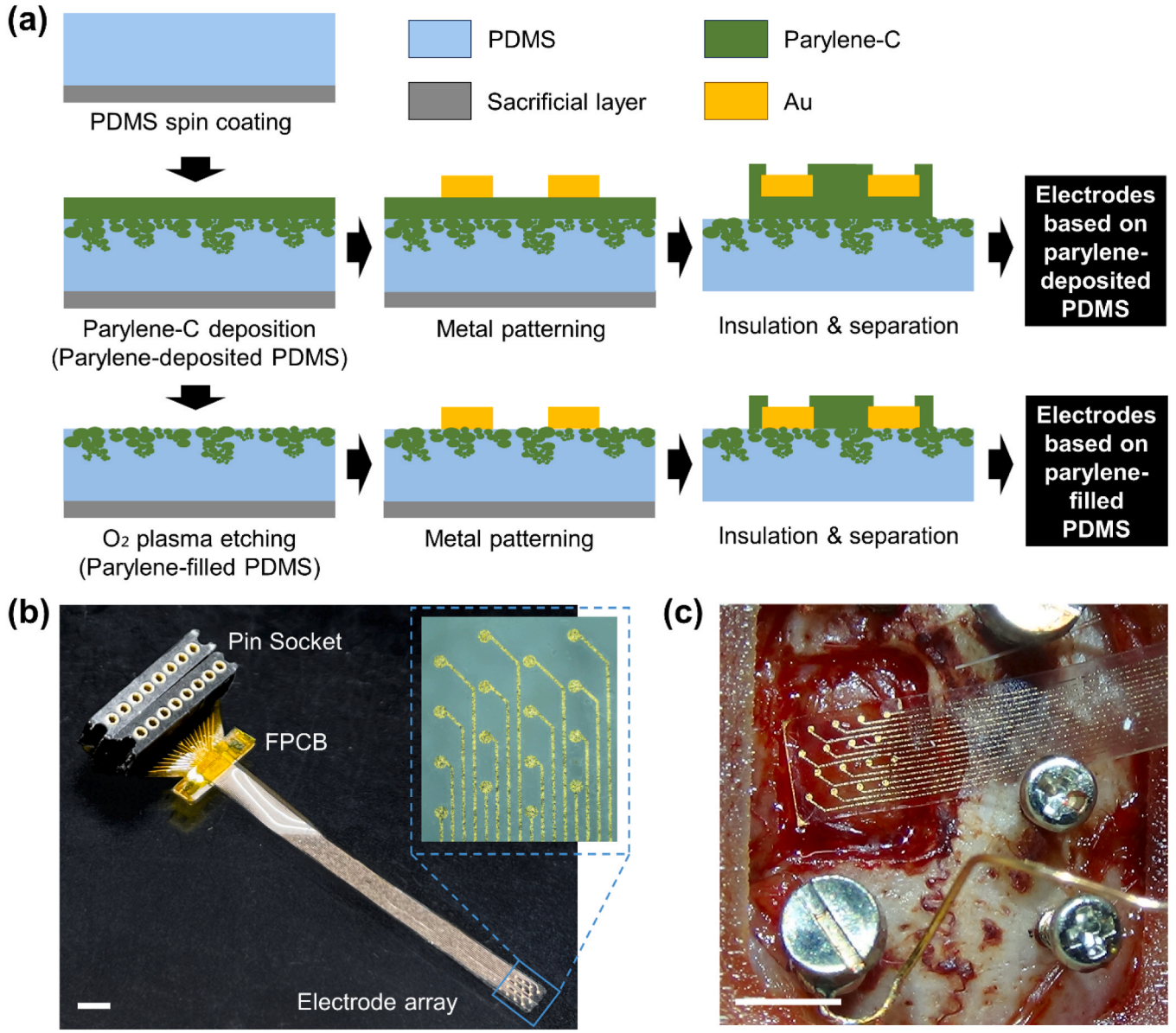

Fig. 1. ECoG electrode array based on PDMS-based substrates treated in two different ways. (a) Fabrication of ECoG electrodes based on surface-treated PDMS substrates: 1. PDMS spin coating, 2. parylene-C deposition resulting in parylene-deposited PDMS, 3. O_2 plasma etching resulting in parylene-filled PDMS, 4. metal patterning, and 5. insulation and separation. The completed ECoG electrode device (b) before and (c) after implantation. Scale bars are 2.5 mm.

and reliability of PDMS-based ECoG electrodes for the first time. Using accelerated aging conditions, the changes in the mechanical and electrochemical properties were monitored over time for up to 8 months. Additionally, the in vivo impedance of the electrodes, which is related to the in vivo recording performance, was investigated over 12 weeks. Somatosensory evoked potentials (SEPs) were successfully recorded in response to mechanical stimuli with various forces for up to 12 weeks using the developed ECoG electrode arrays.

2. Materials and methods

2.1. Fabrication of PDMS-based ECoG electrode arrays

The fabrication steps for the ECoG electrode arrays based on parylene-treated PDMS are illustrated in Fig. 1a. First, poly(acrylic acid) (PAA) was used as a sacrificial layer to avoid mechanical elongation during detachment of the final device. A 5 w/v% PAA solution was spun at 2000 rpm on a 4-in silicon wafer and heated on a hot plate at 95 ℃ for 2 min to vaporize the moisture contained in the solution. The PDMS monomer and curing agent were mixed in a ratio of 1:10 and degassed in a desiccator until bubbles in the mixture completely disappeared. The mixture was spun at 600 and 1250 rpm to obtain PDMS thicknesses of 80 and 150 μm, respectively. Then, it was cured in an oven at 85 ℃ for 1 h. A 1 μm-thick parylene layer was deposited for parylene-deposited PDMS, whereas 400 nm-thick parylene was deposited for parylene-filled PDMS through chemical vapor deposition (NRPC-500, Nuri-Tech Corp., Incheon, Korea). To generate parylene-filled PDMS, reactive ion etching (RIE) was performed at a power of 50 W for 10 min to remove the 400 nm-thick parylene layer from the top surface of the PDMS. The details of fabrication are in Fig. S1.

Titanium (Ti) and gold (Au) with thicknesses of 25 and 200 nm, respectively, were deposited via sputtering (SRN-110, SORONA Inc., Anseong, Korea). Electrode patterns were created by photolithography using a positive photoresist (AZ5214, Merck KGaA, Darmstadt, Germany) and the wet etching of Ti and Au. For insulation, the second parylene layer with 3 μm thickness was deposited and then, RIE at a power of 50 W for 75 min was performed to expose the active electrode sites and contact pads, and to etch the parylene on top of the region outside the metal patterns including electrodes, pads and electrical lines (Fig. S1). Photolithography was performed using a Ti masking layer to expose the desired area. Finally, the edge of the device was manually cut using a scalpel, and the wafer was soaked in deionized water overnight to lift-off the device from the wafer. The fabricated array was connected to a customized flexible printed circuit board (FPCB) using an anisotropic conductive film (ACF) bonder, which could later be joined to a pin socket (Fig. 1b). Consequently, the PDMS-based ECoG electrode array was applied on the brain surface to record SEPs (Fig. 1c).

2.2. Accelerated aging test

Accelerated aging tests were performed following the ASTM F1980 standard to investigate the long-term stability of the developed ECoG electrode array in a mimicked biological environment with an elevated temperature of 57 °C [19,32]. The accelerated aging constants (AAC) for PDMS and parylene were calculated based on the Arrhenius equation (Eq. (1)) and Eq. (2), as follows.

$$k = Ae^{-\frac{E_a}{RT}} \tag{1}$$

where k is the rate constant of chemical reaction and A is the pre-exponential factor, which is slightly affected by temperature; E_a represents the activation energy; R is the universal gas constant; and T is the absolute temperature in Kelvins.

$$AAC = \frac{k_2}{k_1} = \exp\left[\frac{E_a}{k_B}\left(\frac{1}{T_1} - \frac{1}{T_2}\right)\right] \tag{2}$$

where k_1 and k_2 are the rate constants at temperatures T_1 and T_2, respectively; k_B is the Boltzmann's constant; T_1 is the reference temperature of 37 °C; and T_2 is the elevated temperature of 57 °C. The calculated AACs of parylene and PDMS were 2.06 and 1.52, respectively [33–35]. We assumed that a larger AAC may result in faster aging. The experiments were conducted for up to 15 w at 57 °C, which was projected to 31 w at 37 °C, the body temperature.

2.3. Tensile test

Tensile tests were performed using a z-axis stage machine (ESM-303, Mark-10 Corp., Copiague, NY, USA) to measure the mechanical properties. Both sides of the device were fixed to a customized clamp and one side was pulled at a speed of 20 mm/min until the sample fractured (Fig. S2). The tensile strength was measured weekly, using five specimens per sample. To apply the accelerated aging conditions, the samples were immersed in vials containing phosphate-buffered saline (PBS) solution and maintained at 57 °C in an incubator (VS-1203P3V, Visionbionex, Bucheon, Korea). The samples were dried overnight before each tensile test. From the results of the tensile tests, the Young's modulus, E, was extracted from the slope of the strain–stress curve in the elastic region. Moreover, the flexural rigidity was calculated as the product of the Young's modulus and the moment of inertia, which can be obtained from the sample dimensions, as shown in Fig. S3.

2.4. Electrochemical impedance spectroscopy (EIS)

The EIS of the ECoG electrodes was measured using a potentiostat/galvanostat (Reference 600 +, Gamry Instruments, Warminster, PA, USA), employing a three-electrodes setup comprising the working electrode (ECoG electrodes), counter electrode (platinum wire), and reference electrode (Ag/AgCl)) immersed in a PBS solution (Fig. S4). A sinusoidal input with a voltage of 20 mV_{rms} was applied in the frequency range from 10 Hz to 1 MHz. The equivalent circuit model, shown in Fig. 3g, is composed of a resistor due to charge transfer (R_{ct}), coating capacitor (C_c), constant phase element (CPE_{dl}), and Warburg impedance (W_{mt}), which express the electric and ion transfer at the electrolyte–electrode interface. Here, R_s is the solution resistance, whereas CPE_{dl} represents the constant phase element of electric double-layer at the electrode–electrolyte interface, represented by the reciprocal of conductance Y_0 multiplied by $(i\omega)^{-\alpha}$. If α is close to 1, CPE_{dl} acts as a capacitor, whereas if α is close to 0, it acts as a resistor.

2.5. Surgery and device implantation

All surgical procedures for experiments using rats were approved by the Institutional Animal Care and Use Committee (IACUC) of DGIST (Approval No. DGIST-IACUC-21032411–0000). Seven Sprague Dawley rats were used. Before the experiment, two animals were housed in a cage under a standard 12-h light/dark cycle. The rats were anesthetized with isoflurane, and their hair was shaved from the neck to the eyes on the back. To open the skull, the animals were firmly fixed using a stereotaxic instrument. Both eyes were protected from intense light and dry environments during surgery using Vaseline. The scalp was prepared with povidone–iodine solution and 70% ethanol before an incision. The shaved skin was incised along the midline and the exposed skull was wiped with a periosteal elevator to remove the pericranium. The skull and dura mater were opened along the marked line using a hand drill and the opened area was cleaned using saline and cotton swabs. Two steel screws with dimensions of M1.4 × 3 mm were used as the reference and ground electrodes. The screws were soldered using insulated copper wires, and a male-pin connector was mounted on a female header embedded in the printed circuit board (PCB). Holes for the screws were drilled using a hand drill, and the screws were carefully inserted into the hole to avoid penetrating the brain. The ECoG electrode array was

positioned on the brain surface, in the primary somatosensory region (S1). Proper and conformal contacts between the electrodes and brain surface were confirmed through impedance measurements using a signal acquisition equipment (CerePlex Direct, BlackRock Microsystems, Salt Lake City, UT, USA). The implanted area was protected using a shielding cap with dimensions of 14 mm x 12 mm at the bottom and 30 mm x 28 mm at the top with a height of 10 mm, which was made of polycarbonate using a 3D printer (Projet MJP 5500X, 3d Systems, Rock Hill, SC, USA). A piece of the removed skull was placed on the implanted electrode array, and dental resin was applied to fix the shielding cap to the skull.

For surgery on non-human primates, all surgical procedures were approved by the IACUC of KBIOHealth (Approval No. KBIO-IACUC-2022–052–1). Cynomolgus macaque monkeys (*Macaca fascicularis*) weighing 4.5 kg were used in this chronic study. Animals were maintained in an Association for Assessment and Accreditation of Laboratory Animal Care (AAALAC)-approved laboratory animal facility with a standard 12-h light/dark cycle, and had food and water ad libitum. The surgery was performed using standard sterile procedures. After pretreatment with atropine (0.05 mg/kg), anesthesia was induced by an intramuscular injection of ketamine (10 mg/kg) and Xylazine (0.5 mg/kg). After induction, the monkey was intubated and anesthetized with 1–2% isoflurane, and the hair from the neck to eyes on the backside was shaved. Before opening the skull, local lidocaine was applied around the incision line to control bleeding and pain, and the animal was firmly fixed to a stereotaxic instrument. The operative field was disinfected with povidone–iodine solution and 70% ethanol before incision. After skin incision, the muscles and pericranium were scraped to expose the skull. Before opening the skull, the craniotomy site where the device was to be placed was premarked over the motor cortex with approximate coordinates according to the map, and a screw hole was created to reposition and fix the skull. The skull was opened and cleaned with saline solution. The dura mater was gently incised using scissors and then reflected. The ECoG electrode array was placed roughly on the precentral gyrus, at the genus level of the arcuate sulcus, and the cable was fixed to the skull using screws. A customized shielding structure made of stainless steel, to protect the cable, was fixed on the skull using titanium screws. Then, the array was accurately positioned on the targeted S1 region, and the exposed cortical surface and the array were covered with the dura. The bone flap was repositioned over the cranial defect and fixed in place with titanium screws and flexible bioabsorbable bone plates (Inion CPS™ System, INION INC, Weston, FL, USA) on the skull. The muscle and skin were repositioned and the shielding structure and connector were exposed through a separate skin incision. The exposed connector was protected using a lid that was printed with polycarbonate using a 3D printer (Projet 3500 3D Printer, 3d Systems, Rock Hill, SC, USA) and tightened together with the shielding structure using screws when not in use for recording.

2.6. In vivo ECoG recording

SEPs were recorded from the S1 area of rats upon mechanical stimulation of the forelimb and hindlimb using Von Frey hair with at least 100 trials per session (Fig. S8). Signals were recorded at a sampling rate of 30 kHz using a signal acquisition equipment (CerePlex Direct, BlackRock Microsystems, Salt Lake City, UT, USA). The recorded raw signals were processed using a 60 Hz-notch-filter to remove powerline noise and low-pass filtered with a cutoff frequency of 1 kHz.

Chronic in vivo ECoG recordings were performed on cynomolgus monkeys. The ECoG electrode array was integrated with the interconnection part consisting of FPCB cable, PCB board (not visible), Omnetics connector, and shielding structure (Fig. 5b). The reference electrode was positioned beside the recording electrodes and connected through the interconnection part. The ground was connected to the shielding structure that was electrically connected to the fixation screw. Signal recordings and in vivo impedance measurements were performed using an Intan stimulation/recording system (RHS Stim/Recording System, Intan Technologies, Los Angeles, CA, USA). SEPs were recorded from the S1 distal area upon mechanical stimulus of the little finger using Von Frey hairs of 1 g and 10 g. Each stimulation session comprised at least 30 trials. Signals were recorded at a sampling rate of 30 kHz with powerline noise removal using a 60 Hz-notch filter. The recorded data were preprocessed using a bandpass filter from 1 Hz to 1 kHz.

2.7. SEP analysis

The root-mean-square (RMS) noise and signal-to-noise ratio (SNR) were calculated using Eqs. (3) and (4), respectively.

$$\text{Noise\_rms} = \sqrt{\frac{(x_1-\bar{x})^2+(x_2-\bar{x})^2+\cdots+(x_n-\bar{x})^2}{n}} \tag{3}$$

$$\text{SNR} = \frac{V_{pp}}{2\sigma} \tag{4}$$

where x_n represents the recorded value at every data point; $\bar{x}$ represents the mean of the recorded data; n represents the number of recorded data points; V_{pp} represents the peak-to-peak amplitude; and σ represents the RMS value of the noise. A time–frequency analysis was performed, in which the measured SEP signals were decomposed by a complex Morlet wavelet, as defined in Eq. (5).

$$w(t,f_0) = (\sigma_t\pi)^{-1/4} \bullet e^{-\frac{t^2}{2\sigma_t^2}} \bullet e^{2j\pi f_0 t} \tag{5}$$

where t represents each time point of the recorded data; f_0 represents the center frequency; and σ_t represents the width of the wavelet. Referring to previous studies, the constraint ratio was set to $2\pi f_0\sigma_t = 7$ [36,37] and the center frequency used was from 1 to 200 Hz.

3. Results and discussion

3.1. ECoG electrode arrays based on parylene-treated PDMS

We developed soft, conformal ECoG electrode arrays based on two parylene-treated PDMS substrates. Both substrates of parylene-deposited PDMS and parylene-filled PDMS were utilized with different PDMS thicknesses of 80 and 150 μm (Table S1), referred to as samples A–D: parylene-deposited 80 μm-thick PDMS, parylene-deposited 150 μm-thick PDMS, parylene-filled 80 μm-thick PDMS, and parylene-filled 150 μm-thick PDMS, respectively. The completed ECoG device ready for implantation and after implantation are shown in Fig. 1b and c, respectively. The 16-channel ECoG electrodes were arranged in an area of 2.5 × 3 mm^2, with a diameter of 150 μm per electrode and a distance of 600 μm between electrode centers.

3.2. Long-term mechanical properties in accelerated aging condition

Tensile tests were performed to investigate the mechanical properties of the developed ECoG electrode arrays (Fig. 2a). Fig. 2b–e show the strain–stress curves of samples A–D before and after accelerated aging. Before aging (at week 0), the thin substrate with 80 μm PDMS thickness (samples A and C) had higher yield stresses compared with the thick substrate with 150 μm PDMS thickness (samples B and D). Accordingly, the thick PDMS samples exhibited lower Young's moduli (Fig. 2f). In the elastic region, a slightly higher stress was observed for the parylene-deposited PDMS (samples A and B) than for the parylene-filled PDMS (samples C and D); this was due to the existence of a parylene layer on top of the PDMS in the parylene-deposited PDMS samples. In addition, the parylene-filled PDMS had slightly higher stretchability, represented by higher fracture strains, than that of the parylene-deposited PDMS. These results indicate that the initial mechanical properties of the parylene-filled PDMS are closer to those of biological tissues than the

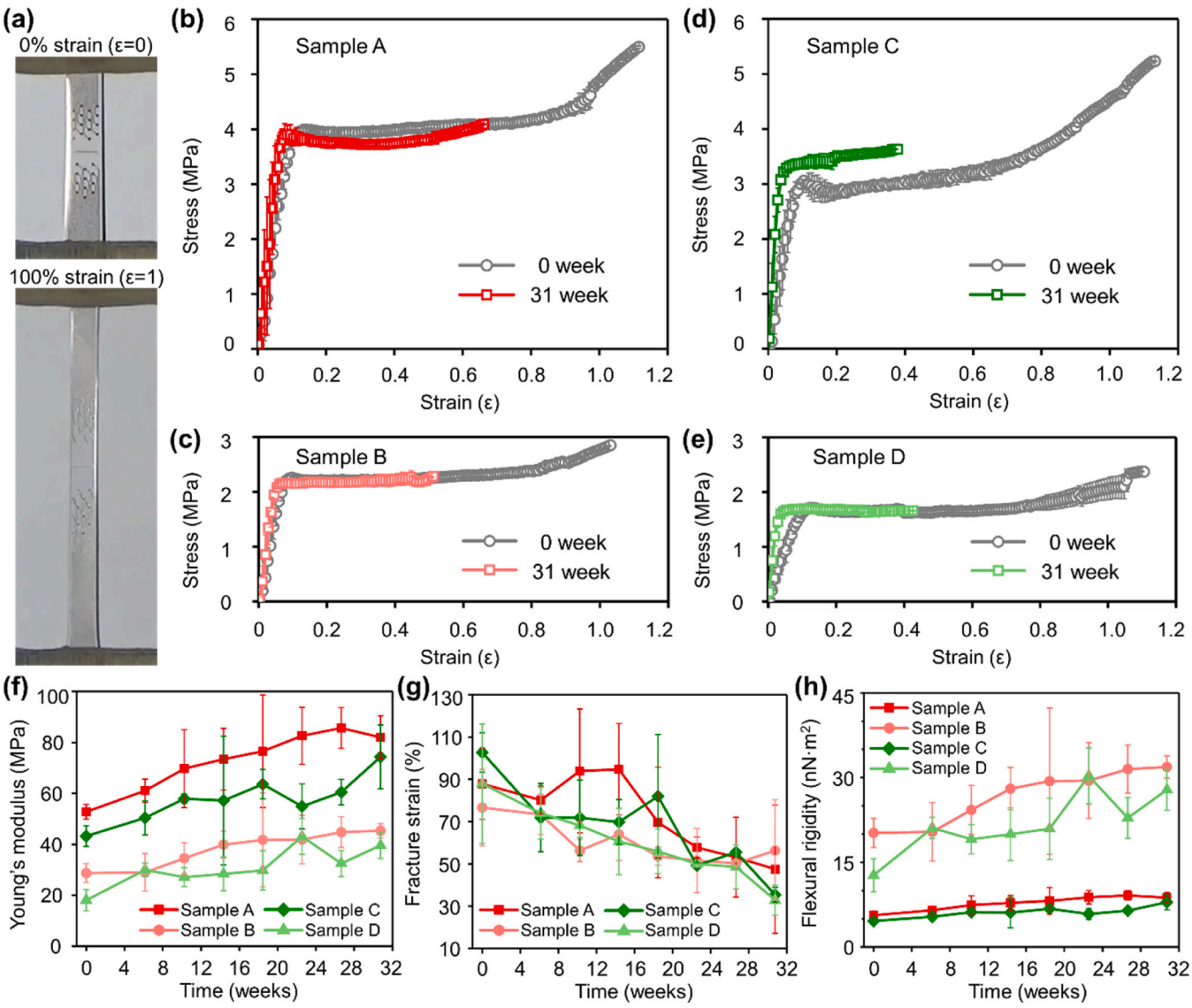

Fig. 2. Long-term mechanical properties of the ECoG electrode arrays based on two differently treated PDMS substrates. (a) Photographs of samples under tensile test, stretched with 0% and 100% strain. (b)–(e) Stress–strain curves of samples A–D, respectively. Gray circles represent measurements before aging, whereas colored squares indicate measurements after aging. Changes in (f) Young's modulus, (g) fracture strain, and (h) flexural rigidity of samples A–D over time up to 31 weeks of accelerated aging ($n \geq 3$).

parylene-deposited PDMS. As summarized in Table S2, our electrodes based on 80 μm-thick parylene-treated PDMS show Young's modulus of 18.1–28.7 MPa, which is much lower than electrodes based on polyimide or parylene (with Young's modulus of a few GPa). Therefore, our device enables conformal contact with the brain surface. Although commercial ECoG devices based on medical-grade silicone have lower Young's modulus (~ 8.28 MPa [38]) than our device, they cannot achieve a conformal contact with the brain surface because of their large thickness (~ 1 mm [39]), thereby causing inflexibility.

Next, the samples were immersed in PBS at 57 °C for accelerated aging (Fig. S2). Compared with the initial stress–strain curves, the Young's moduli increased while the fracture strains decreased for all samples (Fig. 2b–e). The changes in Young's modulus, fracture strain, and bending rigidity over time are summarized in Fig. 2f–h (details in Table S2). The Young's moduli of all samples A–D increased over time, by 55.4%, 57.8%, 72.0%, and 119.3% after 31 weeks, respectively. The parylene-filled PDMS (samples C and D) exhibited larger increases in Young's modulus during aging, which is speculated to be related to more water absorption into PDMS compared with the parylene-deposited PDMS (samples A and B). The Young's modulus of the thick sample D increased more over time than that of the thin sample C, whereas the change in Young's modulus of the parylene-deposited PDMS (samples A and B) was similar regardless of the PDMS thickness. On the other hand, the fracture strains for all samples decreased over time, by 46.0%, 56.3%, 65.6%, and 62.6% for samples A–D, respectively. After aging, stretchability reduced because of water absorption into PDMS. When PDMS swells owing to water, it is easily broken by an external tensile force. In addition, the parylene-deposited PDMS exhibited a smaller decrease in fracture strain than the parylene-filled PDMS. This suggests that the parylene-deposited PDMS is more stable in wet environments thanks to the deposited parylene layer on top of PMDS, which acts as a good barrier against water absorption into PDMS. In terms of flexural rigidity, 150 μm-thick PDMS (samples B and D) had higher flexural rigidity than 80 μm-thick PDMS (samples A and C). In addition, the flexural rigidity increased over time for all samples. In summary, the parylene-filled PDMS had a lower Young's modulus, closer to that of brain tissues, over the entire experimental period, whereas the parylene-deposited PDMS exhibited a slower change in fracture strain over time,

indicating better long-term mechanical stability.

3.3. Long-term electrochemical properties in accelerated aging condition

Fig. 3a and b show the initial EIS results (before aging) for the electrodes based on parylene-deposited PDMS (sample A) and parylene-filled PDMS (sample C), respectively. The impedance at 1 kHz was 222.4 ± 72.3 kΩ for sample A and 27.8 ± 11.2 kΩ for sample C. The significantly lower impedance of sample C was caused by the increased surface area during the etching of parylene from the PMDS surface in the process of creating parylene-filled PDMS. The surface of parylene-filled PDMS was rougher than that of parylene-deposited PDMS as shown in Fig. 3h and i. This enlargement of the surface area where ions can interact with the electrode induces an increase in capacitance, thereby reducing the impedance [40].

To investigate the long-term electrochemical properties of the electrodes, EIS was performed under accelerated aging conditions for 150 days (Fig. S5 and S6). After aging up to 150 days, the impedance at 1 kHz was measured to be 212.37 ± 13.9 kΩ and 55.7 ± 8.5 kΩ for samples A and C, respectively (Fig. 3c and d). Sample A exhibited almost

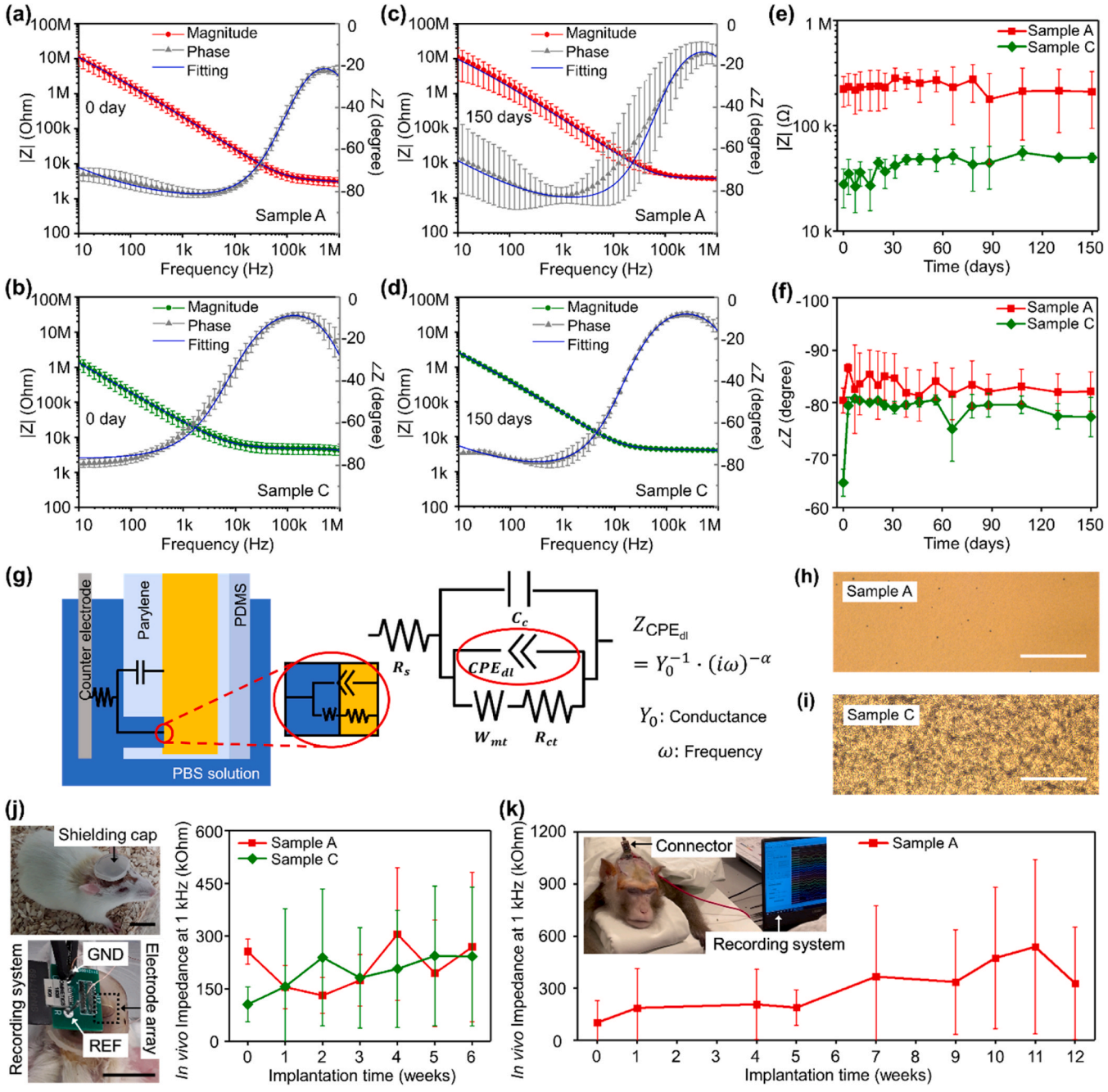

Fig. 3. Long-term electrochemical properties of the ECoG electrodes based on two differently treated PDMS substrates. EIS is measured from the electrodes fabricated based on: (a) and (c) parylene-deposited PDMS (red line); and (b) and (d) parylene-filled PDMS (green line) before and after aging for 150 days ($n \geq 4$), respectively, which is also fitted by curve fitting (blue line) based on the equivalent circuit model. Changes in (e) magnitude and (f) phase of impedance are presented over time for up to 150 days for samples A and C. (g) Equivalent circuit model to describe the electrode-electrolyte interface on the electrode surface. Optical microscopic images of the surfaces of (h) parylene-deposited PDMS and (i) parylene-filled PDMS after Au deposition. The scale bars are 200 μm. In vivo impedance at 1 kHz is obtained over time from the electrodes implanted in (j) the brain of rats ($n \geq 10$) and (k) the brain of non-human primates ($n \geq 20$). The scale bars are 20 mm.

no change in impedance magnitude before and after aging, whereas sample C exhibited doubled impedance magnitude after aging (Fig. 3e, details in Table S3), with the phase for both samples A and C consistently maintained at around –80° (Fig. 3f). Water absorption into the PDMS substrate induced a significant increase in the impedance of sample C. We speculate that the parylene layer deposited on PDMS in sample A acted as an effective barrier against water absorption. Despite the increase in impedance for parylene-filled PDMS, the impedance of the electrodes based on parylene-filled PDMS was four times lower than that of the electrodes based on parylene-deposited PDMS even after aging.

An equivalent circuit model as shown in Fig. 3g was used to analyze the EIS results. As shown in Fig. 3a–d, both the magnitude and phase of the measured impedance were well fitted using the proposed equivalent circuit model before and after aging. As the representative parameters of the equivalent circuit model, the impedance of CPE_{dl} and α, which indicates whether the electrode acts as a capacitor or a resistor, were extracted over time, as shown in Fig. S7a and b, respectively (also Table S3). The result indicates that the capacitive property maintained

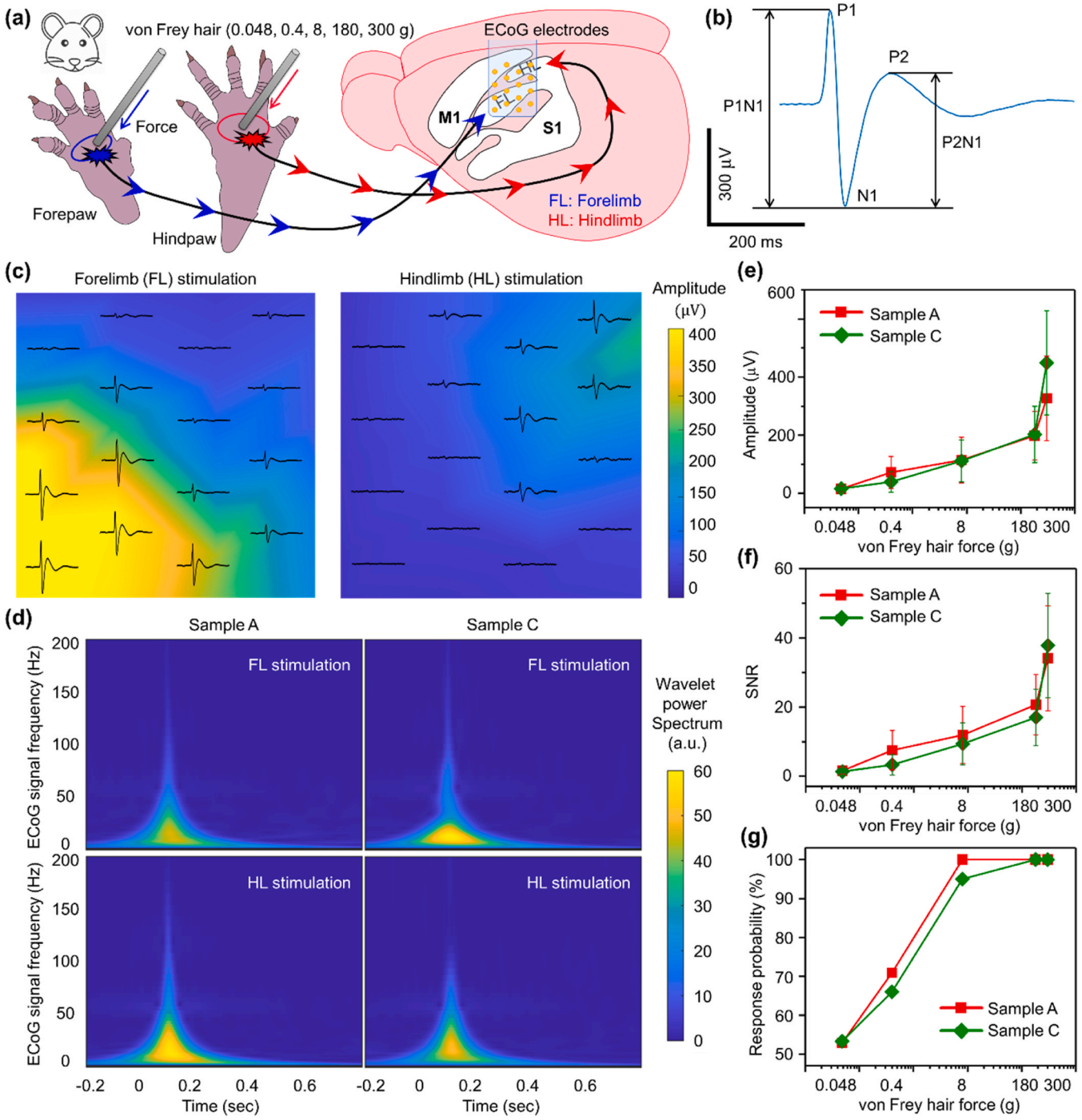

Fig. 4. Recording of SEPs using the ECoG electrode array upon mechanical stimulation on the rat paw. (a) Both forepaw and hindpaw are mechanically stimulated using von Frey hairs with different stiffness, and SEPs are measured from the somatosensory area (S1) related to forelimb (FL) and hindlimb (HL). (b) An example of SEP represents distinctive peaks of P1, N1, and P2. (c) Spatial distributions of evoked SEPs, together with the waveforms of SEPs, are presented according to the location of electrodes in the S1 area. (d) Plots presenting the time–frequency analysis of the SEPs in response to FL and HL stimulation, detected using samples A and C. (e) The amplitude, (f) SNR, and (g) response probability of the SEPs induced by HL stimulation are presented as a function of force applied to the skin, up to 300 g.

consistently for both samples, with alpha being close to one, over the entire experimental period.

3.4. Long-term in vivo impedance

The ECoG electrode arrays based on 80 μm-thick PDMS (samples A and C) were implanted onto the brains of rats, and the in vivo impedance at 1 kHz was monitored over time (Fig. 3j and S8a). The in vivo impedance was measured for 6 weeks in rats and compared with the initial impedance at week 0 (Table S4). The in vivo impedance of samples A and C increased over time (Fig. 3j). A relatively higher increase with larger variance was observed for sample C (parylene-filled PDMS), implying that sample C was likely more affected by the biological environment. In addition, sample A (parylene-deposited PDMS) was also used to measure the in vivo impedance from the brain of non-human primates for up to 12 weeks (Fig. 3k). The impedance increased slightly until week 5, similar to the results obtained in the rat brain; however, a dramatic increase in impedance was observed afterward (Table S5). Although the in vivo impedance was increased to more than 500 kΩ, it enabled the recording of SEP signals.

3.5. Recording of somatosensory evoked potentials

The ECoG electrodes based on samples A and C were used to record SEPs in response to mechanical stimuli in rat paws (Fig. S8). The SEPs acquired from the left somatosensory cortex by poking the right paw using a von Frey hair (Fig. 4a), which provided information on the quantitative force applied, clearly detected the signal peaks of P1, N2, and P2 (Fig. 4b). The ECoG arrays based on samples A and C recorded similar SEPs induced by mechanical stimulation (Fig. S9). Moreover, we demonstrated that a specific cortical area could be identified upon stimulation of the forelimb (FL) or hindlimb (HL) through brain mapping based on evoked SEPs (Fig. 4c). The brain maps, which overlapped with the averaged SEPs, exhibited high-amplitude signals in different regions depending on either FL or HL stimulation. These responsive regions were consistent with the cortical areas known to be associated with FL or HL. To evaluate the recording performance of the electrodes based on parylene-treated PDMS, the evoked SEPs were further analyzed in terms of time–frequency analysis, amplitude, noise level, and SNR. The time–frequency plots show the frequency components of brain activity, such as delta (1–3 Hz), theta (4–7 Hz), alpha (8–12 Hz), beta (14–30 Hz), low gamma (35–50 Hz), and high gamma (>60 Hz) components in the time domain (Fig. 4d). High gamma signals associated with cognition were detected around the N1 peak.

SEPs were detected in response to forces applied to the hindpaw at various levels ranging from 0.048 to 300 g. The amplitude of the evoked SEPs increased gradually up to a force of 180 g, after which a dramatic increase was observed at a force of 300 g (Fig. 4e). Accordingly, the SNR also increased with the signal amplitude (Fig. 4f). The response probability, which indicates the probability of whether a SEP response is induced by a mechanical stimulus, was almost 100% with a force over 8 g (Fig. 4g). The amplitude, SNR, and response probability are summarized in Table S6. In summary, no significant difference was observed in the recording performance of samples A and C. However, when stimulated using a large force of 300 g, sample C exhibited a relatively higher signal amplitude and SNR, thus indicating slightly better performance in in vivo recording (Fig. 4e and f). SEPs evoked by mechanical stimulation of paws with a force of 300 g showed that the amplitudes of P1N1 and P2N1 measured using sample C were observed to be larger by 48.5% and 37.3% than using sample A, respectively, resulting in a higher SNR (Fig. S10).

To evaluate the long-term applicability of the developed ECoG array, we recorded SEPs from a cynomolgus macaque monkey for 12 weeks. While von Frey hairs with forces of 1, 10, and 180 g were applied to the fingertip of digit five (D5) and the center region of the palm, SEPs were recorded from the hand region of the S1 (Fig. 5a and b). To target the hand region of the S1 in monkeys, the ECoG array was optimized so that the number of recording electrodes was increased to 32 to cover the target area. The 80 μm-thick parylene-deposited PDMS (Sample A) was used as the substrate for electrodes. The active site of the electrodes was 200 μm in diameter, and the center-to-center distance between the electrodes was 1.25 mm.

Fig. 5c shows that different amplitudes of SEPs were observed upon stimulus with different forces of 1 g and 180 g to the palm. In addition, we clearly identified two distinct locations responding to the stimulus applied to the D5 fingertip and palm by recording SEPs from different electrode channels (Fig. 5d). Based on the brain atlas [41,42], our recordings of SEPs from different locations corresponded to the known S1 areas of the digits and palm (Fig. 5e). However, the finger region identified from our recordings was wider than that reported in previous studies, which may indicate that the method used to provide mechanical stimulation cannot specifically stimulate the fingertip but also stimulate adjacent regions around the target point. In addition, individual differences between subjects may have contributed to differences in the size of the responsive cortical areas.

SEPs were successfully recorded for 12 weeks. Fig. S11a shows examples of the signals recorded from all 32 channels at week 0, 5, and 12. The background noise level varied depending on the anesthetic status and the recording circumstance, even the recording condition was strictly controlled. We analyzed the SEPs upon mechanical stimulus of 10 g applied to the D5 fingertip. As shown in Fig. 5f, SEPs were consistently obtained from the left central region of the electrode array over 12 weeks. The amplitude of SEPs gradually increased until week 5, presumably due to the environmental modification of the tissue around the ECoG electrodes caused by the recovery after implantation. Fig. S11b shows the SEPs obtained at week 1, 5, 7, and 12. At week 5, the SEP amplitude detected was maximum, with an averaged and maximum amplitudes of 201 μV and 335 μV, respectively, and then gradually decreased up to week 7. Afterward, the SEP amplitude remained consistently until week 12 (Fig. 5g). Even though the amplitude of SEPs changed over time, we were able to record brain activity for a long period.

We detected SEPs as the stimulus strength increased using von Frey hairs of 1, 10, and 180 g (Fig. S12a–c, respectively). The SEP waveforms were similar in that a positive peak appeared first, followed by a negative peak, regardless of stimulus strength (Fig. S12a–c). The averaged amplitude of SEPs in response to 1, 10, and 180 g stimulus was 210, 264, and 327 μV, respectively, at week 5 (Fig. 5h). Even at week 12, the SEP amplitude with 10 g stimulation was higher than that with 1 g stimulation (Fig. S12e). The SEPs with high-strength stimuli exhibited oscillations after the main spike (Fig. S12d). We analyzed the SEPs using the normalized power spectral density (PSD) (Fig. 5i and S12f). In all frequency bands of the brainwaves, the stimulus using 180 g exhibited the highest power among the three stimulation strengths. The normalized power gradually increased with the stimulus strength in the alpha, beta, and gamma bands. A previous study reported that tactile sensations can be produced by electrical stimulation of low-frequency bands from the alpha to gamma bands [43]. The recorded brain activities showed the same frequency bands as in the previous study, thereby proving that our electrodes can discriminate the sensational changes and stimulation strength. Exceptionally, the SEP signals induced by only 180 g of stimulus, a high-strength stimulation, exhibited high energy in the theta band, which was not observed in SEPs induced by lower-strength stimulations.

Since the differences in stimulation methods, active site properties (e.g., coating materials and active area), and recording regions, the major frequency band from evoked PSDs is hard to compare. Nevertheless, the maximum value of PSD is one of the factors to compare the quality of recording performance. Fig. S13 shows the PSDs from our developed ECoG array in (a) and previously reported electrodes in (b) [44–47]. The maximum power in PSD recorded by our electrodes was from 20 to 30 dB, which is comparable to that of previously reported

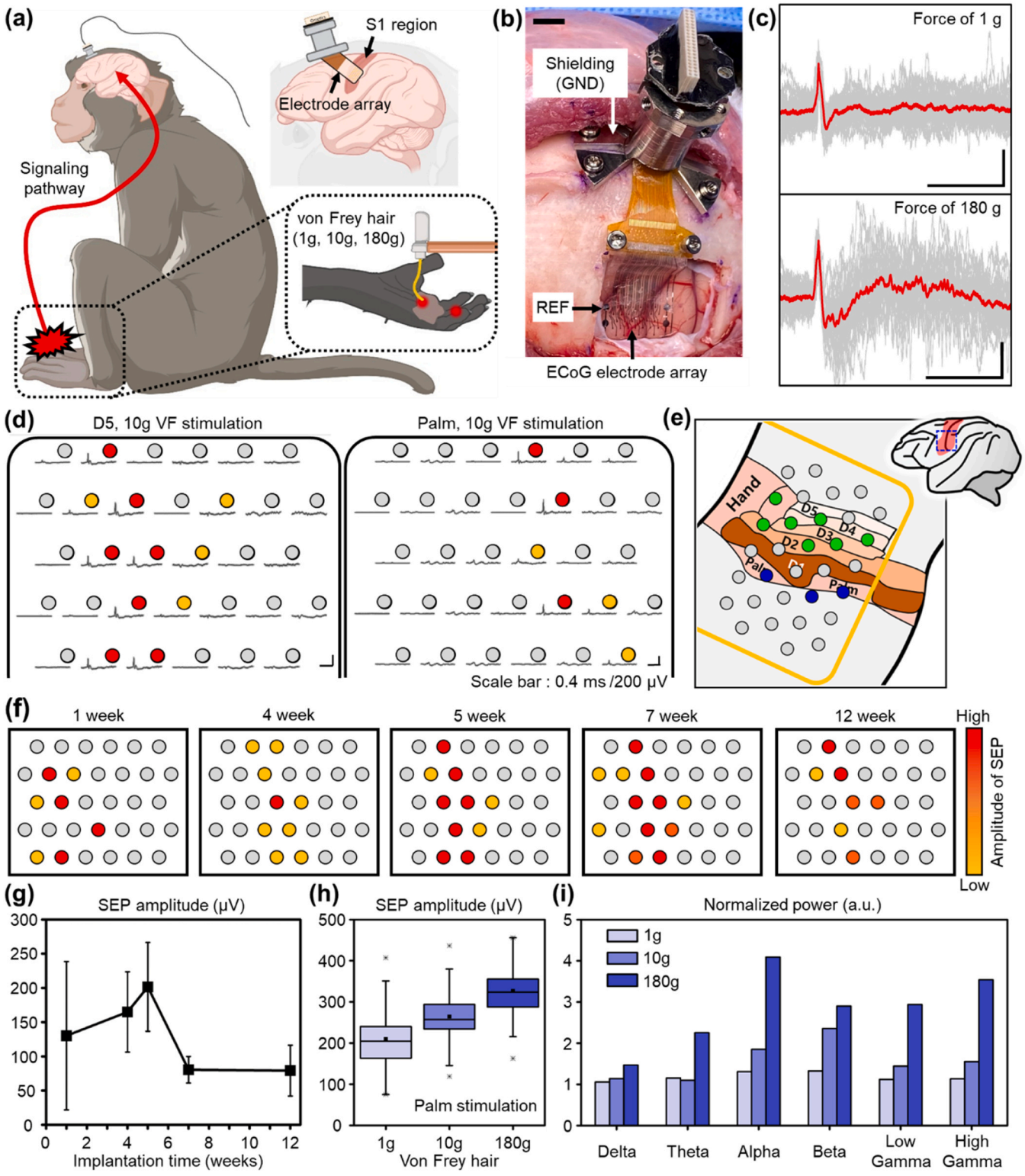

Fig. 5. Recording of SEPs using the ECoG electrode array upon mechanical stimulation on the skin of a monkey. (a) Schematic illustration of chronic SEP recording. [Illustration was created with BioRender.com.] (b) Photograph of an EcoG electrode array implanted on the hand region of the primary somatosensory cortex (S1). A shielding structure was fixed on the skull using screws connected to the ground. The scale bar is 5 mm. (c) Recorded SEPs with different pressure levels applied to the palm. The scale bars indicate 0.2 s in time and 100 μV in amplitude. (d) Spatial distribution of SEPs evoked by a force of 10 g applied to the D5 fingertip and the center of the palm. (e) Locations of the electrodes along with the atlas of the monkey brain. The electrodes that recorded SEPs evoked by D5 and palm stimulation are highlighted in green and blue, respectively. (f) Spatial distribution of evoked SEPs over 12 weeks. (g) Amplitude of SEPs, induced by a force of 10 g applied to D5 fingertip over time. (h) Amplitude of SEPs as a function of the applied force from 1 to 180 g, measured at week 5. (i) Based on power spectral density analysis, the frequency components of the SEPs measured at week 5 are compared with different stimulus strengths.

ECoG electrodes, from 20 dB to 40 dB [44–48]. In our experiment, the value of PSDs under 20 Hz was increased by tactile stimulus using von Frey hairs as shown in Fig. S13a, clearly showing that the power of SEPs was increased by tactile stimulus. Although the nature of recorded brain responses was different, the recording performance of the developed electrodes in the low-frequency band was similar to the previously published results showing the increase in PSD during seizure events [44, 46]. At high frequencies above 100 Hz, the signals detected by our electrodes exhibited higher power than previously reported ECoG signals. As the result, our developed ECoG devices exhibited the recording quality in frequency domain comparable to previously reported custom-developed [44,46–48] and commercial ECoG arrays [45].

In previous studies [45,47,49], long-term ECoG recordings were mostly conducted using commercial ECoG electrodes, which are based on medical-grade silicone and have electrode dimensions in millimeter scale (Table S7). In comparison with commercial and previously developed silicone-based electrodes, our PDMS-based device showed higher SNR, as summarized in Table S7. Normally, the frequency range of ECoG analysis was up to 200 Hz. The PSD of our recorded ECoG signals in the given bandwidth was similar with those reported in previous ECoG results [45,47,49]. Furthermore, the maximum signal power from the PSD of our device was comparable to those of previously reported electrodes. On the other hand, only a few studies using micro-ECoG electrodes have reported long-term recording results, such as in [20,22,50]. In comparison with those micro-ECoG electrodes, our electrodes based on parylene-treated PDMS show higher SNR as shown in Table S7. As summarized in Table S7, our PDMS-based electrodes have electrode dimensions in micrometer scale, but at the same time, show long-term ECoG recording performance comparable with previously reported silicone-based electrodes including commercial devices. It is attributed to the soft and flexible nature of our developed device, with a much smaller thickness (80 μm) than that of silicone-based electrodes (ca. 10 times thicker and thus, almost inflexible).

4. Conclusion

We investigated the long-term mechanical and electrochemical properties of PDMS-based ECoG electrode arrays, and validated their recording performance in in vivo. Initially, electrodes on parylene-filled PDMS exhibited better mechanical and electrical performance compared with electrodes on parylene-deposited PDMS, as they possessed a lower Young's modulus, lower bending rigidity, higher stretchability, and lower impedance. However, electrodes on parylene-deposited PDMS exhibited better mechanical and electrical stability over time compared with those on parylene-filled PDMS. In parylene-deposited PDMS, the thin parylene layer effectively suppressed water uptake into PDMS and minimized the effects of the wet environment. However, electrodes based on parylene-filled PDMS were also suitable for long-term use as the impedance remained consistently low over the entire experimental period of up to 5 months. In vivo experiments demonstrated that the developed PDMS-based ECoG arrays could record SEPs chronically over months. In summary, both parylene-deposited and parylene-filled PDMS, which are compatible with MEMS fabrication processes, can be used as soft and flexible substrates for long-term implantable devices. Our results suggest the potential of PDMS-based bioelectronic devices for various applications requiring softness, flexibility, conformability, and device robustness over long-term.

CRediT authorship contribution statement

Hyunmin Moon: Data curation, Investigation, Methodology, Validation, Visualization, Writing – original draft. **Jae-Won Jang:** Data curation, Formal analysis, Investigation, Methodology, Visualization, Writing – original draft. **Sumi Park:** Data curation, Formal analysis, Investigation, Methodology, Validation, Visualization. **Joong-Hyun Kim:** Methodology, Resources, Writing – original draft. **June Sic Kim:** Funding acquisition, Methodology, Validation, Writing – review & editing. **Sohee Kim:** Conceptualization, Funding acquisition, Project administration, Resources, Supervision, Validation, Writing – review & editing.

Declaration of Competing Interest

The authors declare that they have no known competing financial interests or personal relationships that could have appeared to influence the work reported in this paper.

Data availability

Data will be made available on request.

Acknowledgements

This work was supported by grants from the National Research Foundation (NRF) of Korea (NRF-2018M3C7A1022309 and NRF-2019R1A2C1009674), and from DGIST (21-RT-01), funded by the Ministry of Science and ICT of Korea. The authors would like to thank the Institute of Next-generation Semiconductor Convergence Technology and Laboratory Animal Resource Center at DGIST.

Appendix A. Supporting information

Supplementary data associated with this article can be found in the online version at doi:10.1016/j.snb.2023.135099.

References

[1] J.H. Lee, H. Kim, J.H. Kim, S.H. Lee, Soft implantable microelectrodes for future medicine: prosthetics, neural signal recording and neuromodulation, Lab Chip 16 (2016) 959–976.
[2] R. Vakani, D.R. Nair, Chapter 20 - Electrocorticography and functional mapping, in: K.H. Levin, P. Chauvel (Eds.), Handbook of Clinical Neurology, Elsevier, 2019, pp. 313–327.
[3] M. Shokoueinejad, D.W. Park, Y.H. Jung, S.K. Brodnick, J. Novello, A. Dingle, et al., Progress in the Field of Micro-Electrocorticography, Micromachines 10 (2019) 62.
[4] N. Lago, A. Cester, Flexible and organic neural interfaces: a review, Appl. Sci. 7 (2017) 1292.
[5] G. Buzsaki, C.A. Anastassiou, C. Koch, The origin of extracellular fields and currents - EEG, ECoG, LFP and spikes, Nat. Rev. Neurosci. 13 (2012) 407–420.
[6] T. Araki, F. Yoshida, T. Uemura, Y. Noda, S. Yoshimoto, T. Kaiju, et al., Long-term implantable, flexible, and transparent neural interface based on Ag/Au Core-Shell Nanowires, Adv. Healthc. Mater 8 (2019) 1900130.
[7] C. Bohler, M. Vomero, M. Soula, M. Voroslakos, M. Porto Cruz, R. Liljemalm, et al., Multilayer Arrays for Neurotechnology Applications (MANTA): chronically stable thin-film intracortical implants, Adv. Sci. 10 (2023), e2207576.
[8] F. Fallegger, G. Schiavone, E. Pirondini, F.B. Wagner, N. Vachicouras, L. Serex, et al., MRI-Compatible and conformal electrocorticography grids for translational research, Adv. Sci. 8 (2021) 2003761.
[9] F. Zhang, L. Zhang, J. Xia, W. Zhao, S. Dong, Z. Ye, et al., Multimodal electrocorticogram active electrode array based on zinc oxide-thin film transistors, Adv. Sci. 10 (2023), e2204467.
[10] A.R. Hassan, Z.F. Zhao, J.J. Ferrero, C. Cea, P. Jastrzebska-Perfect, J. Myers, et al., Translational organic neural interface devices at single neuron resolution, Adv. Sci. 9 (2022) 2202306.
[11] C.Y. Chen, M.M. Xue, Y.G. Wen, G. Yao, Y. Cui, F.Y. Liao, et al., A ferroelectric ceramic/polymer composite-based capacitive electrode array for in vivo recordings, Adv. Healthc. Mater 6 (2017) 1700305.
[12] M. Du, S. Guan, L. Gao, S. Lv, S. Yang, J. Shi, et al., Flexible micropillar electrode arrays for in vivo neural activity recordings, Small 15 (2019), e1900582.
[13] K.D. Xu, S.J. Li, S.R. Dong, S.M. Zhang, G. Pan, G.M. Wang, et al., Bioresorbable electrode array for electrophysiological and pressure signal recording in the brain, Adv. Healthc. Mater. 8 (2019) 1801649.
[14] Q. Zhao, M. Zhu, G. Tian, C. Liang, Z. Liu, J. Huang, et al., Highly sensitive and omnidirectionally stretchable bioelectrode arrays for in vivo neural interfacing, Adv. Healthc. Mater. 12 (2023), e2203344.
[15] D. Yan, A.A. Jiman, E.C. Bottorff, P.R. Patel, D. Meli, E.J. Welle, et al., Ultraflexible and stretchable intrafascicular peripheral nerve recording device with axon-dimension, cuff-less microneedle electrode array, Small 18 (2022), e2200311.
[16] K. Scholten, E. Meng, Materials for microfabricated implantable devices: a review, Lab Chip 15 (2015) 4256–4272.

[17] R. Dong, L. Wang, C. Hang, Z. Chen, X. Liu, L. Zhong, et al., Printed stretchable liquid metal electrode arrays for in vivo neural recording, Small 17 (2021), e2006612.
[18] I.R. Minev, P. Musienko, A. Hirsch, Q. Barraud, N. Wenger, E.M. Moraud, et al., Electronic dura mater for long-term multimodal neural interfaces, Science 347 (2015) 159–163.
[19] K. Oh, D. Byun, S. Kim, Polymer-based interconnection cables to integrate with flexible penetrating microelectrode arrays, Biomed. Micro 19 (2017) 76.
[20] A.F. Renz, J. Lee, K. Tybrandt, M. Brzezinski, D.A. Lorenzo, M.C. Cheraka, et al., Opto-E-Dura: a soft, stretchable ECoG array for multimodal, multiscale neuroscience, Adv. Healthc. Mater 9 (2020) 2000814.
[21] G. Schiavone, F. Fallegger, X.Y. Kang, B. Barra, N. Vachicouras, E. Roussinova, et al., Soft, implantable bioelectronic interfaces for translational research, Adv. Mater. 32 (2020) 1906512.
[22] K. Tybrandt, D. Khodagholy, B. Dielacher, F. Stauffer, A.F. Renz, G. Buzsaki, et al., High-density stretchable electrode grids for chronic neural recording, Adv. Mater. 30 (2018) 1706520.
[23] H. Moon, N. Chou, H.W. Seo, K. Lee, J. Park, S. Kim, Transformation of 2D Planes into 3D soft and flexible structures with embedded electrical functionality, ACS Appl. Mater. Inter. 11 (2019) 36186–36195.
[24] K. Izdihar, H.R. Abdul Razak, N. Supion, M.K.A. Karim, N.H. Osman, M. Norkhairunnisa, Structural, mechanical, and dielectric properties of polydimethylsiloxane and silicone elastomer for the fabrication of clinical-grade kidney phantom, Appl. Sci. 11 (2021) 1172.
[25] P. Fattahi, G. Yang, G. Kim, M.R. Abidian, A review of organic and inorganic biomaterials for neural interfaces, Adv. Mater. 26 (2014) 1846–1885.
[26] H. Moon, B. Park, D. Hong, K.S. Park, S. Lee, S. Kim, 3D-structured soft bioelectronic devices with crack-free metal patterns, Sens. Actuat. B Chem. 343 (2021), 130123.
[27] N. Chou, J. Jeong, S. Kim, Crack-free and reliable lithographical patterning methods on PDMS substrate, J. Micromech. Microeng. 23 (2013), 125035.
[28] N. Chou, H. Moon, J. Park, S. Kim, Interfacial and surface analysis of parylene C-modified PDMS substrates for soft bioelectronics, Prog. Org. Coat. 157 (2021), 106309.
[29] H. Moon, S. Kim, Soft and flexible 3D-structured device with crack-free metal patterns, Proc. IEEE Int. Conf. Micro Electro Mech. Syst. (MEMS) (2020) 245–248.
[30] K.Y. Lee, H. Moon, B. Kim, Y.N. Kang, J.W. Jang, H.K. Choe, et al., Development of a polydimethylsiloxane-based electrode array for electrocorticography, Adv. Mater. Interfaces 7 (2020) 2001152.
[31] J. Jeong, N. Chou, S. Kim, Long-term characterization of neural electrodes based on parylene-caulked polydimethylsiloxane substrate, Biomed. Micro 18 (2016) 42.
[32] Y.N. Kang, N. Chou, J.W. Jang, D. Byun, H. Kang, D.J. Moon, et al., An intrafascicular neural interface with enhanced interconnection for recording of peripheral nerve signals, IEEE T. Neur. Sys. Reh. 27 (2019) 1312–1319.
[33] D.W.L. Hukins, A. Mahomed, S.N. Kukureka, Accelerated aging for testing polymeric biomaterials and medical devices, Med. Eng. Phys. 30 (2008) 1270–1274.
[34] W. Chun, N. Chou, S. Cho, S. Yang, S. Kim, Evaluation of sub-micrometer parylene C films as an insulation layer using electrochemical impedance spectroscopy, Prog. Org. Coat. 77 (2014) 537–547.
[35] J.E. Mark, Polymer Data Handbook, Oxford University Press,, New York, NY, USA, 2009.
[36] S. Herculano-Houzel, C. Watson, G. Paxinos, Distribution of neurons in functional areas of the mouse cerebral cortex reveals quantitatively different cortical zones, Front. Neuroanat. 7 (2013) 35.
[37] H. Oya, H. Kawasaki, M.A. Howard, R. Adolphs, Electrophysiological responses in the human amygdala discriminate emotion categories of complex visual stimuli, J. Neurosci. 22 (2002) 9502–9512.
[38] I. Rachinskiy, L. Wong, C.H. Chiang, C. Wang, M. Trumpis, J.I. Ogren, J. Viventi, High-density, actively multiplexed μECoG array on reinforced silicone substrate, Front. Nanotechnol. 4 (2022), 837328.
[39] S.V. Hiremath, E.C. Tyler-Kabara, J.J. Wheeler, D.W. Moran, R.A. Gaunt, J. L. Collinger, W. Wang, Human perception of electrical stimulation on the surface of somatosensory cortex, PloS One 12 (2017), e0176020.
[40] Z.F. Zhao, G.D. Spyropoulos, C. Cea, J.N. Gelinas, D. Khodagholy, Ionic communication for implantable bioelectronics, Sci. Adv. 8 (2022), eabm7851.
[41] A.M.H. Seelke, J.J. Padberg, E. Disbrow, S.M. Purnell, G. Recanzone, L. Krubitzer, Topographic Maps within Brodmann's Area 5 of Macaque Monkeys, Cereb. Cortex 22 (2012) 1834–1850.
[42] S. Harding-Forrester, D.E. Feldman, Chapter 4 - Somatosensory maps, in: G. Vallar, H.B. Coslett (Eds.), Handbook of Clinical Neurology, Elsevier, 2018, pp. 73–102.
[43] M. Feurra, W. Paulus, V. Walsh, R. Kanai, Frequency specific modulation of human somatosensory cortex, Front. Psychol. 2 (2011) 13.
[44] X. Li, Y. Song, G. Xiao, E. He, J. Xie, Y. Dai, Y. Xing, Y. Wang, Y. Wang, S. Xu, M. Wang, T.H. Tao, X. Cai, PDMS–Parylene hybrid, flexible micro-ECoG electrode array for spatiotemporal mapping of epileptic electrophysiological activity from multicortical brain regions, ACS Appl. Bio Mater. 4 (2021) 8013–8022.
[45] E.S. Nurse, S.E. John, D.R. Freestone, T.J. Oxley, H. Ung, S.F. Berkovic, T. J. O'Brien, M.J. Cook, D.B. Grayden, Consistency of long-term subdural electrocorticography in humans, IEEE Trans. Biomed. Eng. 65 (2017) 344–352.
[46] K.D. Xu, S.J. Li, S.R. Dong, S.M. Zhang, G. Pan, G.M. Wang, L. Shi, W. Guo, C.N. Yu, J.K. Luo, Bioresorbable electrode array for electrophysiological and pressure signal recording in the brain, Adv. Healthc. Mater 8 (2019) 1801649.
[47] T.F. Yan, K. Suzuki, S. Kameda, M. Maeda, T. Mihara, M. Hirata, Electrocorticographic effects of acute ketamine on non-human primate brains, J. Neural Eng. 19 (2022), 026034.
[48] H. Yang, Z.Y. Qian, J.J. Wang, J.Y. Feng, C.Q. Tang, L.Y. Wang, Y. Guo, Z.W. Liu, Y. Q. Yang, K.L. Zhang, P.N. Chen, X.M. Sun, H.S. Peng, Carbon nanotube array-based flexible multifunctional electrodes to record electrophysiology and ions on the cerebral cortex in real time, Adv. Funct. Mater. 32 (2022) 2204794.
[49] C. Larzabal, S. Bonnet, T. Costecalde, V. Auboiroux, G. Charvet, S. Chabardes, F. Sauter-Starace, Long-term stability of the chronic epidural wireless recorder WIMAGINE in tetraplegic patients, J. Neural Eng. 18 (2021), 056026.
[50] V. Woods, M. Trumpis, B. Bent, K. Palopoli-Trojani, C.H. Chiang, C. Wang, C. Yu, M.N. Insanally, R.C. Froemke, J. Viventi, Long-term recording reliability of liquid crystal polymer μECoG arrays, J. Neural Eng. 15 (2018), 066024.

Hyunmin Moon received the B.S. degree in biomedical engineering from Gachon University, Incheon, Korea in 2012. He received the M.S. and Ph.D. degrees in robotics engineering from Daegu Gyeongbuk Institute of Science and Technology (DGIST), Daegu, Korea in 2014 and 2021, respectively. From 2021–2023, he was a Postdoctoral Researcher with the Department of Robotics and Mechatronics Engineering, DGIST. Since 2023, he has been a Postdoctoral Researcher with the Department of Mechanical Engineering, Massachusetts Institute of Technology (MIT), Boston, MA, USA. His research interests include neural interfaces for brain and peripheral nerve applications as well as soft bioelectronics employing robust, conductive, and bioadhesive hydrogels.

Jae-Won Jang received the B.S. degree in electrical engineering from Kyungpook National University, Daegu, Korea in 2017. He is a Ph.D. candidate in robotics and mechatronics engineering from Daegu Gyeongbuk Institute of Science and Technology (DGIST), Daegu, Korea. His research interests include neural interfaces for brain applications using hard and soft materials.

Sumi Park received the B.S. degree in mechanical engineering from Pukyoung National University, Busan, Korea in 2020. She received the M.S. degree in robotics and mechatronics engineering from Daegu Gyeongbuk Institute of Science and Technology (DGIST), Daegu, Korea in 2022. Since 2022, she has been working as an engineer with Samsung Electronics, Korea.

Joong-Hyun Kim received the D.V.M., M.S., and Ph.D. degrees in veterinary medicine from Chungbuk National University, Cheongju, Korea, in 2001, 2003, and 2007, respectively. He worked with the Veterinary Teaching Hospital, Department of Veterinary Surgery, Chungbuk National University. From 2007–2009, he was a Postdoctoral Researcher with the Department of Biomedical Engineering and Imaging, University of Tennessee Health Science Center, Memphis, TN, USA, and the Department of Restorative Dentistry, University of Texas Health Science Center, Houston, TX, USA. He was a Research Professor with Dankook University, Cheonan, Korea, from 2009 to 2016, and with Jeonbuk National University, Jeonju, Korea, from 2016 to 2017. Since 2017, he has been a Senior Researcher with the Non-Clinical Evaluation Center, Osong Medical Innovation Foundation, Cheongju, in charge of medical device evaluation. He also currently works as an Attending Veterinarian. His research interests include tissue engineering for musculoskeletal systems including oral tissue and dental biomaterials.

June Sic Kim received the B.S. degree in electrical engineering and the M.S. and Ph.D. degrees in biomedical engineering from Hanyang University, Seoul, Korea, in 1996, 1998, and 2002, respectively. He worked with the Montreal Neurological Institute, McGill University, Montreal, QC, Canada, from 2002 to 2004, as a Postdoctoral Researcher. He worked as an Assistant Professor with the Department of Neurosurgery, Seoul National University, Seoul, Korea from 2004 to 2014. Since 2014, he has been working as a Research Professor with the Institute of Basic Sciences, Seoul National University. He is interested in brain-computer interfaces based on neuroimage and electrophysiology.

Sohee Kim received the B.S. and M.S. degrees in mechanical engineering from Korea Advanced Institute of Science and Technology (KAIST), Daejeon, Korea, in 1998 and 2000, respectively, and the Dr.-Ing. (Ph.D.) degree in mechatronics from the University of Saarland, Saarbruecken, Germany, in 2005. She worked with the Fraunhofer Institute for Biomedical Engineering (IBMT), St. Ingbert, Germany, as a Researcher. From 2006–2009, she was a Postdoctoral Researcher in electrical and computer engineering with the University of Utah, Salt Lake City, UT, USA. From 2009–2015, she was a Professor with the Gwangju Institute of Science and Technology (GIST), Gwangju, Korea, in both the Departments of Medical System Engineering and Mechatronics. Since 2015, she has been a Professor with the Department of Robotics and Mechatronics Engineering, Daegu Gyeongbuk Institute of Science and Technology (DGIST), Daegu, Korea. Her research interests include neural interfaces for brain, retina, and peripheral nerve applications as well as polymer-based soft MEMS technologies and flexible/wearable devices for biomedical applications.